Available online at www.sciencedirect.com
SCIENCE DIRECT®
Journal of Power Sources 139 (2005) 304–313
JOURNAL OF POWER SOURCES
www.elsevier.com/locate/jpowsour

Differential voltage analyses of high-power lithium-ion cells 2. Applications

Ira Bloom[a,*], Jon Christophersen[b], Kevin Gering[b]

[a] *Electrochemical Technology Program, Argonne National Laboratory, 9700 South Cass Avenue, Argonne, IL 60439, USA*
[b] *Idaho National Engineering and Environmental Laboratory, P.O. Box 1625, Idaho Falls, ID 83415, USA*

Received 28 June 2004; accepted 20 July 2004
Available online 17 September 2004

Abstract

We characterized high-power lithium-ion cells in terms of performance and cycle- and calendar life at 45 °C. Among other parameters, we measured the C/25 capacity every 4 weeks during the test. Differentiation of the C/25 voltage versus capacity data with respect to capacity yielded dV/dQ curves. Analysis of Q_0 dV/dQ curves has shown that capacity fade in high-power lithium-ion cells can be complex. From the analysis, the anode material in a significant fraction of the cells showed two types of capacity loss. The loss of accessible material tended to happen early in cell life, either during formation or during the first 4 weeks of testing. Most likely this was caused by a physical rather than chemical process. After 4 weeks, the principal cause of capacity loss was side reactions.

Keywords: Differential voltage; Reference electrode; Lithium ion; Battery

1. Introduction

Lithium-ion batteries are considered ideal where applications require high specific or volumetric energy or power densities. High-power lithium-ion batteries are also being considered for use in automotive applications by the U.S. Department of Energy-supported Freedom Cooperative Automotive Research, FreedomCAR, Partnership. The batteries usually consist of a lithiated metal oxide positive (cathode), such as $LiCoO_2$, $LiMn_2O_4$, or $LiNiO_2$, a carbon negative (anode) and a lithium salt dissolved in an organic electrolyte.

Two national laboratories, Argonne National Laboratory (ANL) and Idaho National Engineering and Environmental Laboratory (INEEL), collaborated to understand the causes of resistance rise and capacity and power fade in lithium-ion batteries [1]. This work showed that the C/25 capacity was proportional to $t^{1/2}$. The trend in the resistance and power data also depended on $t^{1/2}$.

Some of the C/25 data were presented in an earlier paper [2] to describe and demonstrate the use of differential voltage (dV/dQ) curves to elucidate some of the fade mechanisms in lithium-ion batteries. The dV/dQ curves permitted easy graphical analysis, whereas using differential capacity curves (dQ/dV) was more problematic. Phenominologically speaking, the peaks in the dV/dQ curves are from phase transitions, whereas the peaks in the dQ/dV curves are from phase equilibria. At phase equilibria, two or more coexisting phases with different lithium concentrations have the same lithium chemical potential. Thus, dV = 0 at phase equilibria and the value of dQ/dV is undefined. On the other hand, with a constant current discharge (or charge) to generate the data, dQ is always nonzero.

The peaks in the dV/dQ curves were assigned to the cathode, the anode, or their sum by comparison to half-cell data. The paper showed how to apply the dV/dQ techniques to un-

* Corresponding author. Tel.: +1 630 252 4516; fax: +1 630 252 4176.
E-mail address: bloom@cmt.anl.gov (I. Bloom).

0378-7753/$ – see front matter © 2004 Elsevier B.V. All rights reserved.
doi:10.1016/j.jpowsour.2004.07.022

derstand a simple case. We showed that the capacity fade is primarily due to side reactions at the anode. In the work that follows, we will continue the discussion and show how to use dV/dQ curves in a more complicated case where there is evidence of complex phenomena occurring at the anode. These phenomena were observed in both the calendar- and cycle-life experiments.

2. Experimental

2.1. 18650-sized cells

Detailed information regarding cell construction is given in [1]. The testing regime is described in [1–4]. The cell chemistry is given in Table 1. The average active area was 846.3 cm^2 and the nominal C/1 capacity was 0.8 Ah. Twenty-six weld-sealed, 18650-sized cells were fabricated to ANL's specifications for this work. The cells underwent formation cycles before delivery to ANL and INEEL. After characterization at 25 °C, one cell was removed from testing at both ANL and INEEL. This left only 10 cells at ANL (calendar life) and 14 at INEEL (cycle life) for testing at 45 °C.

The cells were characterized in terms of their charge and discharge C/25 capacities before the tests began. After 4 weeks at temperature, the cells were cooled to 25 °C and reference performance tests (RPTs) were performed. The RPTs consisted of portions of the characterization tests, including the C/25 tests. The cells were then heated to the soak temperature. The process was repeated until the power fade at the 300 Wh line was greater than 50%. See [3,4] for more information regarding the test procedures and test plan.

Table 1
Cell chemistry

Cathode electrode
8 wt.% PVDF binder (Kureha KF-1100)
4 wt.% SFG-6 graphite (Timical)
4 wt.% carbon black (Chevron)
84 wt.% $LiNi_{0.8}Co_{0.1}Al_{0.1}O_2$
8 mg/cm^2 loading density
35 μm thick coating/side
30 μm thick Al current collector
Anode electrode
8 wt.% PVDF binder (Kureha #C)
92 wt.% MAG-10 (Hitachi)
4.9 mg/cm^2 loading density
35 μm thick coating/side
18 μm thick Cu current collector
Electrolyte
1.2 M $LiPF_6$ in EC/EMC (3:7 by weight)
Separator
25 μm thick Celgard 2325 separator

Table 2
Distribution of number of peaks in cell population

No. of peaks	Count	Percent of population
1	18	75
2	6	25
Total	24	

2.2. Half cells

Half-cell construction from fresh and aged 18650 materials was described previously [2,5]. The half cells were charged and discharged at the C/25 rate. The charge and discharge voltages were measured and recorded every 30 s. This yielded about 2500–4800 data points for analyses.

2.3. Data reduction and calculations

As described earlier [2], the C/25 charge and discharge data for the cells from each test population as well as the half cells were noisy due to the very slow charge/discharge rates. Mathematical filtering was used to average out the noise and accentuate the peaks. The filtering was performed using Microsoft Excel and consisted of calculating the percentage depth-of-discharge (%DOD) for each point based on the experimental data and then using the FORECAST function to interpolate the cell capacity and voltage at evenly spaced %DOD intervals. Typically, 0.5% DOD intervals were used, yielding 200 points for subsequent manipulation and plotting. $-Q_0\,dV/dQ$ was calculated as $-Q_0 \times \Delta V/\Delta(\text{Ah})$, where Q_0 is the measured C/25 capacity of the cells (in Ah), Δ(Ah) the change in the capacity of a cell in a given interval and ΔV the change in cell voltage as a result of Δ(Ah). The Q_0 factor served to normalize the derivatives based on cell capacity. Further smoothing of $-Q_0\,dV/dQ$ was accomplished by using a 5-point moving average. Plots of $-Q_0\,dV/dQ$ versus capacity density (mAh/cm^2) were then analyzed for trends.

In the half-cell work, full-cell potentials were calculated by subtracting the anode potential from that of the cathode. Similarly, the full-cell derivatives were calculated as the differences between those of the cathode and the anode. For the electrode slippage calculation, the electrode alignments relative to each other were shifted from left to right in terms of which section of the total electrode capacity was actually used in the cell. The cell capacity was defined as that between the voltage limits of 4.1 and 3.0 V.

Before comparing the 18650- and half-cell data, the 18650-cell data was shifted relative to the data from the anode half cell. The active area was also decreased. This aligned the voltage versus capacity discharge curves of the two types of cells. Once the adjustments were made, they were not changed.

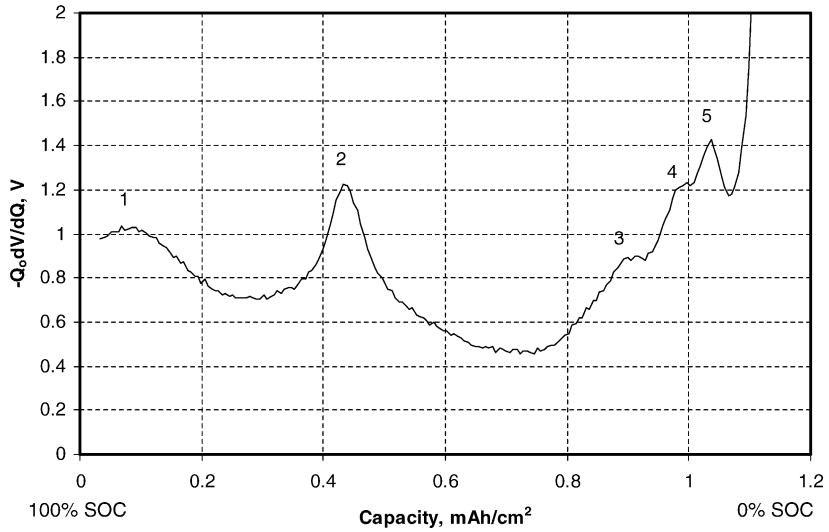

Fig. 1. Example of a type 1 $-Q_0\,dV/dQ$ vs. capacity plot at $t = 0$ weeks (discharge only). The SOC convention used in this figure is implicit in the rest of this paper. The initial C/25 capacity of this cell was 0.96 Ah.

3. Results and discussion

An examination of the $-Q_0\,dV/dQ$ plots at $t = 0$ weeks shows that they fall into two main categories: one peak between 0.3 and 0.5 mAh/cm^2 (type 1; Fig. 1) and two peaks in this capacity range (type 2; Fig. 2). The distribution of the types of plots is given in Table 2. From the data in Table 2, it can be seen that there are more type 1 plots in the population than type 2 plots.

In the previous work [2], a comparison of half cell and 18650 data was made. The results of the half-cell work served as a basis for assigning the peaks in Fig. 1 to the cathode, anode or a combination of them. Those results showed that peak 1 is from the cathode only. Peak 2 is a mixture of cathode and anode peaks, but it is mostly from the anode. Peaks 3–5 are from the anode.

With these results as a basis, the peaks in Fig. 2 can be assigned analogously based on their positions. That is, peak 1 is from the cathode only. Peaks 2a and 2b are due to the cathode and anode, but mostly due to the anode; and peak 3 is due to the anode.

A reason why there are two peaks can be found if the possibility of nonuniformity in the anode material is considered. During cell construction, the anodes were manufactured from an *N*-methylpyrrolidinone slurry containing the PVdF binder and MAG-10 graphite. After an initial drying step, the electrode was laminated onto the copper current collector/backing plate in a calendaring process. Since MAG-10 is a flaky form of graphite (see Fig. 3A), the alignment of the grains and the space between them were affected by the calendaring process. Indeed, in Fig. 3A grains appear to be preferentially aligned. In Fig. 3B, there are two configurations

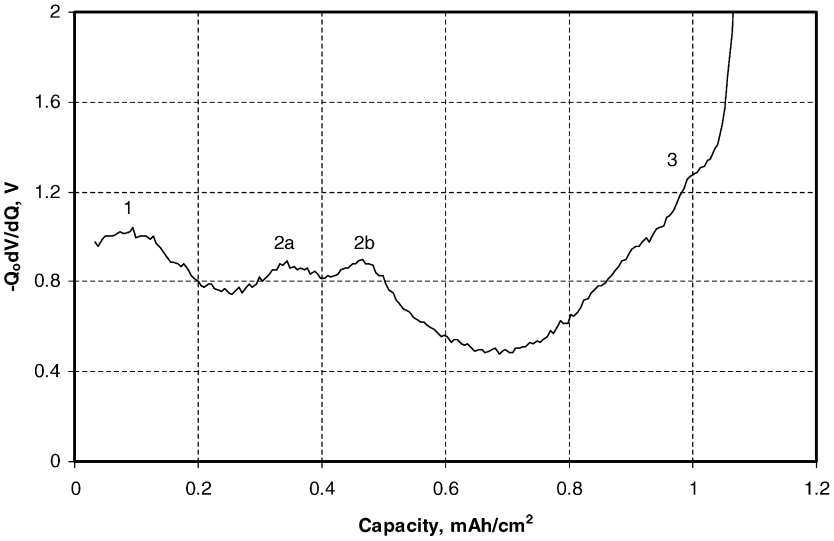

Fig. 2. Example of a type 2 $-Q_0\,dV/dQ$ plot at $t = 0$ weeks (discharge only). The initial C/25 capacity of this cell was 0.94 Ah.

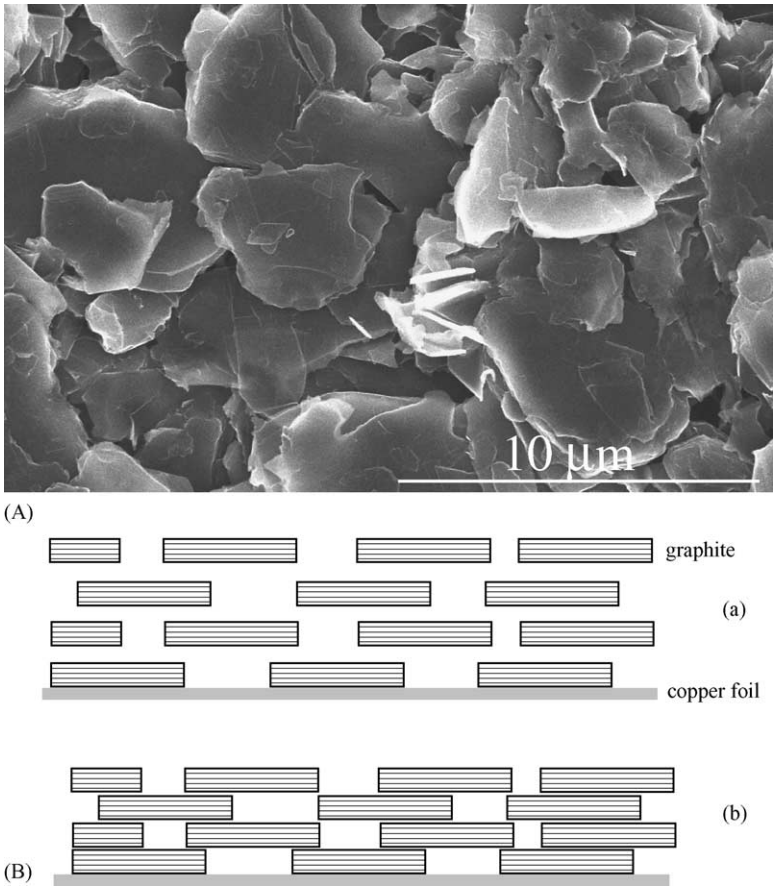

Fig. 3. (A) Scanning electron micrograph of MAG-10 graphite; (B) schematic illustration of graphite particle alignment on copper foil current collector. Configuration "a" allows relatively facile lithium diffusion to the graphite particles, while "b" hinders it.

of the graphite particles, "a" and "b". In both, the graphene layers are parallel to the copper foil current collector. It is expected that lithium diffusion perpendicular into the graphene layers is very slow compared to diffusion parallel into the layers, and will be ignored for this discussion. Configuration "a" allows relatively facile lithium diffusion from the electrolyte to the space between the graphene layers. In "b", access to the graphene layers is restricted due to the longer, more tortuous path for lithium diffusion, which hinders lithium diffusion and intercalation. For the sake of simplicity, the particles in configuration "a" will be referred to as "I", and those in "b" will be referred to as "II".

Ordinarily, the effect of graphene layer accessibility would be expected only at high discharge rates. It would not be expected at the low rates used in this work. However, the work of Aurbach et al. [6] has shown the effect of pressure on the capacity and morphology of flaky graphite electrodes. Aurbach et al. used three electrodes: unpressed, pressed to 5×10^3 kg/cm^2, and pressed by the wheels on a rolling machine. In his cyclic voltammetry experiments, the scan rates varied from 5 to 50 μV/s for the 0–0.3 V window (the 10 μV/s scan rate would take about 8.3 h to complete; this rate is similar to the C/25 rates used in our tests). The pressed and rolled anodes displayed significantly lower capacities than the unpressed one. Pressure, from both pressing and rolling, was found to orient the basal planes parallel with the collector and pack the particles tighter than in the unpressed case, with the rolled case being more tightly packed than the pressed case. Pressure can also come from other sources. For example, in another paper [7], Aurbach et al. report that, in electrode materials with a large number of crevices in the edge planes, the pressure due to the deposition of electrolyte reduction products can cause the graphite particles to crack during the early cycles. Another source of pressure comes from inserting the rolled cell structure into the 18650 can off-center. The nonuniformity of physical pressure in either of these cases may cause some of the particles in I to move to II.

In an electrode consisting of both I and II configurations (I + II), if there were a sufficiently large population of II, the net effect would be that one section of the anode would behave as if it had a lower capacity, and phase transitions in II would occur at a correspondingly lower capacity. In Fig. 4a, a schematic illustration of this situation is plotted as potential versus the concentration of lithium (c_{Li}). Particles in configuration I follow curve "a"; those in II follow curve "b". At equilibrium, the potentials of I and II are equal, as shown by the horizontal line in Fig. 4a. Here, the values

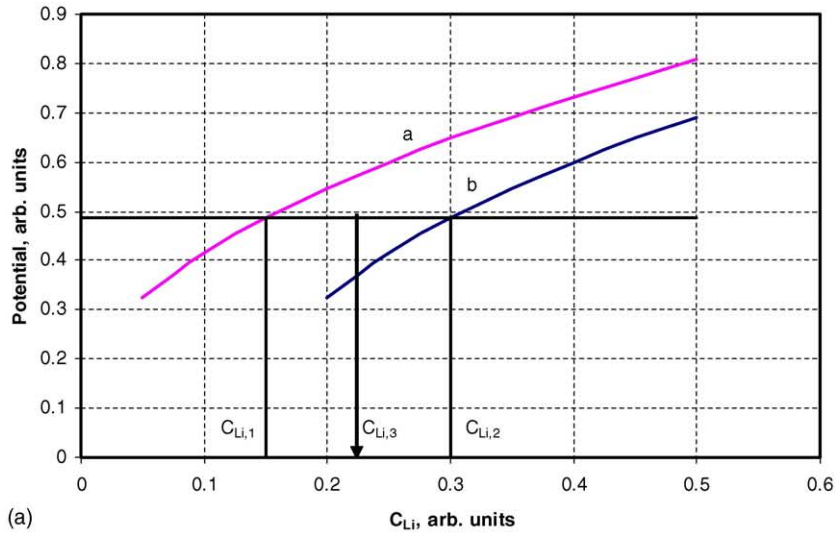
Potential, arb. units
a
b
$C_{Li,1}$
$C_{Li,3}$
$C_{Li,2}$
C_{Li}, arb. units

(a)

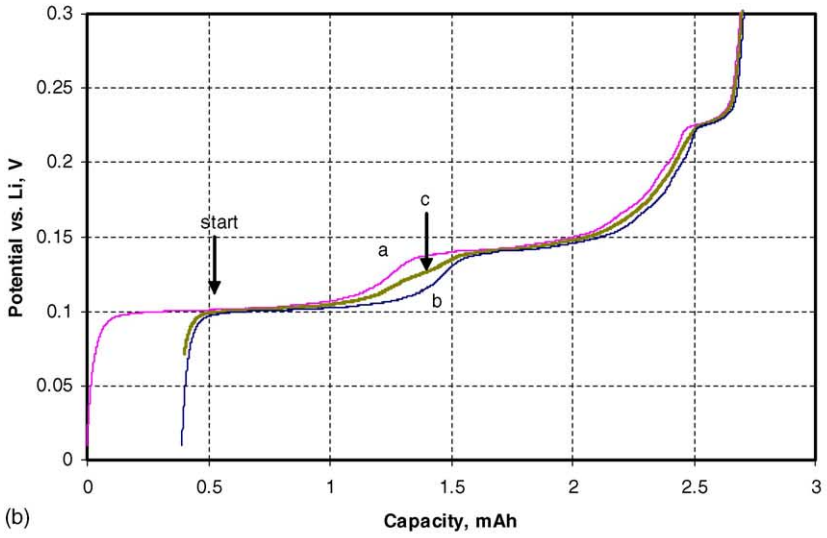
Potential vs. Li, V
start
a
b
c
Capacity, mAh

(b)

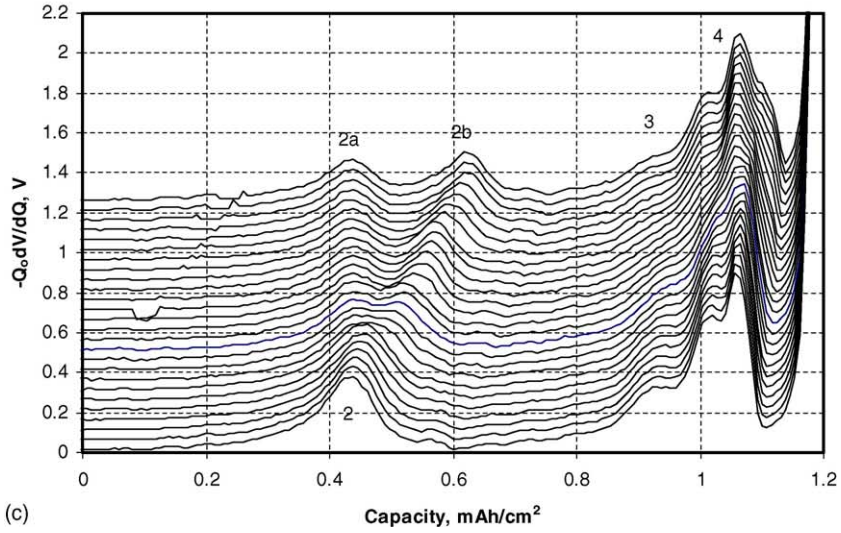
$-Q_o dV/dQ$, V
2
2a
2b
3
4
Capacity, mAh/cm^2

(c)

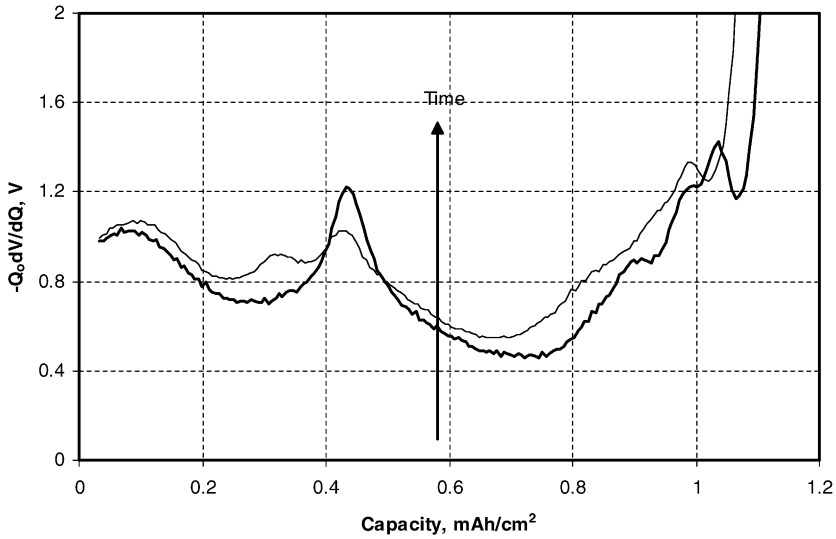

Fig. 5. Plot of $-Q_0\,\mathrm{d}V/\mathrm{d}Q$ vs. capacity from an 18650 cell, showing the anode peak at ~0.45 mAh/cm^2 becoming two peaks. The t = 0 week curve is bolded for the sake of clarity. Note that there is some shifting of the t = 4 week curve due to cell capacity fade.

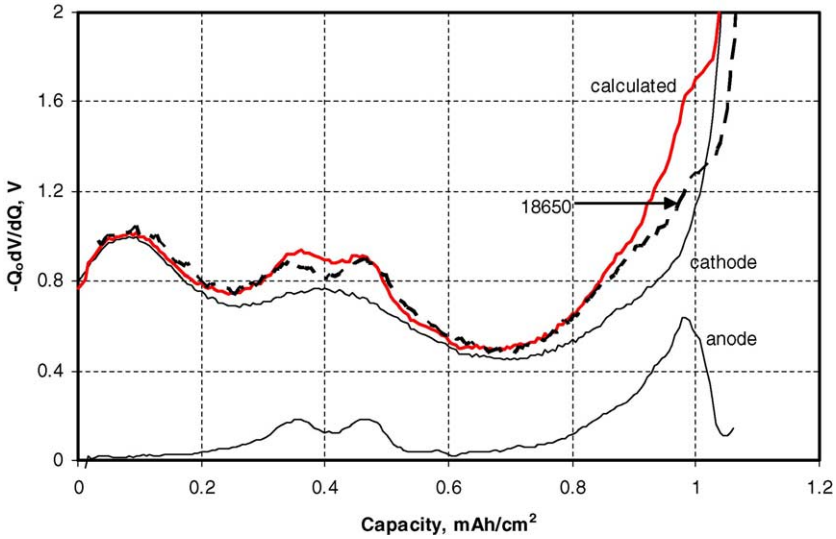

Fig. 6. Plot of the $-Q_0\,\mathrm{d}V/\mathrm{d}Q$ curves from an 18650 cell with those calculated from anode and cathode half cells and their sum.

of c_{Li} which correspond to the equilibrium potential are indicated as $c_{\mathrm{Li},1}$ and $c_{\mathrm{Li},2}$, respectively, for the two curves. In the I + II electrode, the concentration of lithium at this equilibrium potential, $c_{\mathrm{Li},3}$, is between $c_{\mathrm{Li},1}$ and $c_{\mathrm{Li},2}$. This argument is similar to the lever rule (graphical rendering of a material balance) used in phase diagrams. The exact value of $c_{\mathrm{Li},3}$ depends on the relative amounts of $c_{\mathrm{Li},1}$ and $c_{\mathrm{Li},2}$ in the composite electrode.

To a first-order approximation, capacity is linearly related to c_{Li}. One can readily see that the principles described above carry over to plotting the data on a capacity axis. In the real anode, let us assume that the particles in I follow the potential versus capacity curve "a" (see Fig. 4b) and that the particles in II, which have lost accessible capacity, follow curve "b" when the anode is discharged. At equilibrium, the potentials of the two particle groups are equal, but II would be at a higher

Fig. 4. (a) Equilibrium potential vs. concentration of lithium in the anode (c_{Li}) showing how to find the concentration of lithium when the two curves interact in a simple case. (b) Potential vs. capacity of the anode when nonuniform fade is present. Curve "a" represents the starting material; curve "b", an area that has lost active material; curve "c", an equally weighted mixture of the two. (c) Calculated $-Q_0\,\mathrm{d}V/\mathrm{d}Q$ vs. capacity for the I + II anode. The curves in this plot have been shifted so that the features in the bottommost curve align with those in Fig. 1 and shows peak 2 splitting into peaks 2a and 2b with capacity fade of the II part of the anode. The numbering scheme of the bottommost curve is the same as that in Fig. 1. A vertical displacement has been added for the sake of clarity. Capacity fade in the II part of the anode increases vertically from 0 to 25% in steps of 1%.

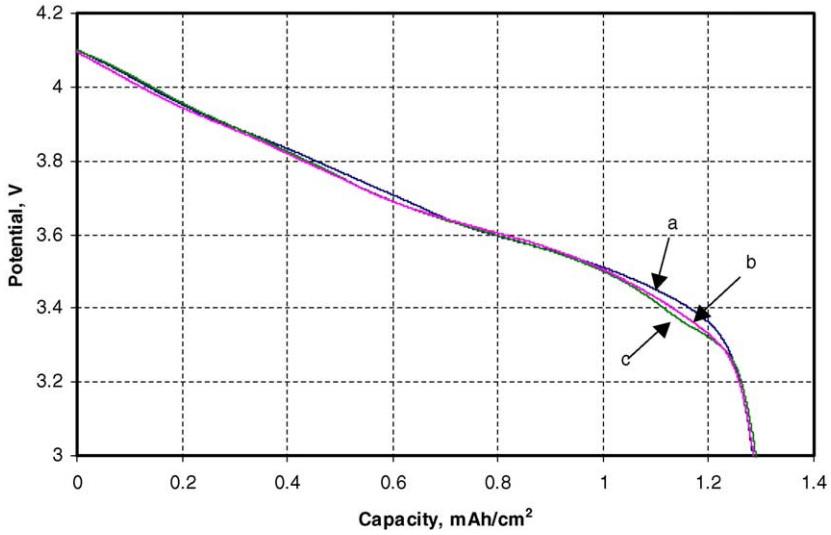

Fig. 7. Potential vs. capacity curves for three cells. Curve "a" is the calculated discharge curve for a cell with a homogeneous anode; curve "b" is the calculated discharge curve for a cell with a I + II anode; curve "c" is the discharge curve for the 18650 cell. The amount of relative shift between the anode and cathode for curves "a" and "b" is the same.

state-of-charge than I, for example, at the position marked "start" in Fig. 4b. The voltage versus capacity curve for the I + II anode is represented by curve "c" and was derived by using an equally weighted mixture of "a" and "b".

Using the mixing scheme outlined above and keeping the proportions of I and II arbitrarily fixed at 1:1, potential versus capacity curves were calculated for cases in which the II part of the mixed electrode lost from 0 to 25% of its accessible capacity. From these calculations and after differentiating with respect to capacity, the resulting $-Q_0\,dV/dQ$ curves, given in Fig. 4c, show the effect of loss of accessible capacity on the shape of $-Q_0\,dV/dQ$ curve. As the loss of accessible capacity increases, peak 2 in Fig. 4c seems to divide into peaks 2a and 2b. A closer inspection of the positions of peaks 2 and 2a shows that they are the same peak. With increased loss of accessible material, the separation between peaks 2a and 2b increases and the separation of peak 2b and peaks 3 and 4 decreases.

Indeed, evidence of the separation of peaks phenomena was seen in some of the $-Q_0\,dV/dQ$ curves from the 18650 cells. In the $-Q_0\,dV/dQ$ data from two cells, there was one peak at $t = 0$ weeks and two peaks at $t = 4$ weeks. An example of this is given in Fig. 5. Thus, the loss of accessible active material occurs early in cell life, either during the formation process or during the first 4 weeks of testing.

The series of $-Q_0\,dV/dQ$ curves in Fig. 4c was used to select which curve should be used in subsequent calculations of the voltage versus capacity curve for the cell. By comparing the separation of peaks 2a and 2b (0.12 mAh/cm^2) in Fig. 2 with those in Fig. 4c, the $-Q_0\,dV/dQ$ curves representing a

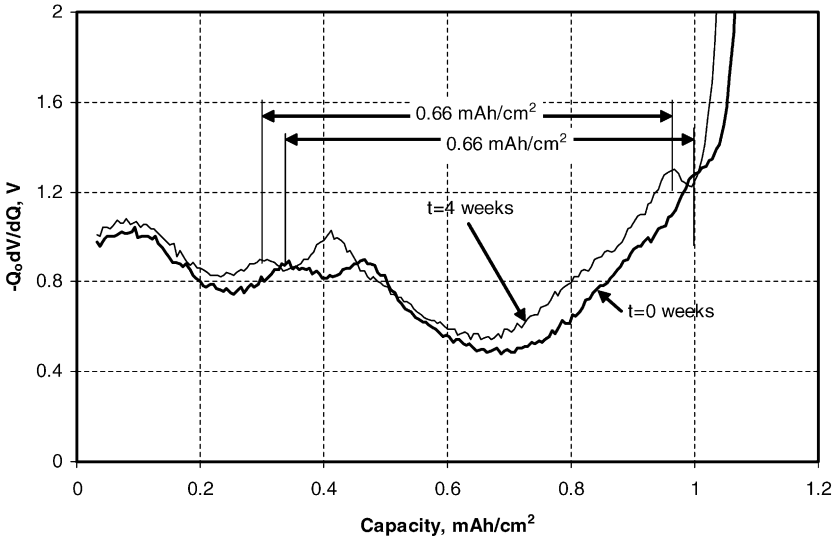

Fig. 8. Initial aging of an 18650 cell ($t = 0$ week data were shown in Fig. 2).

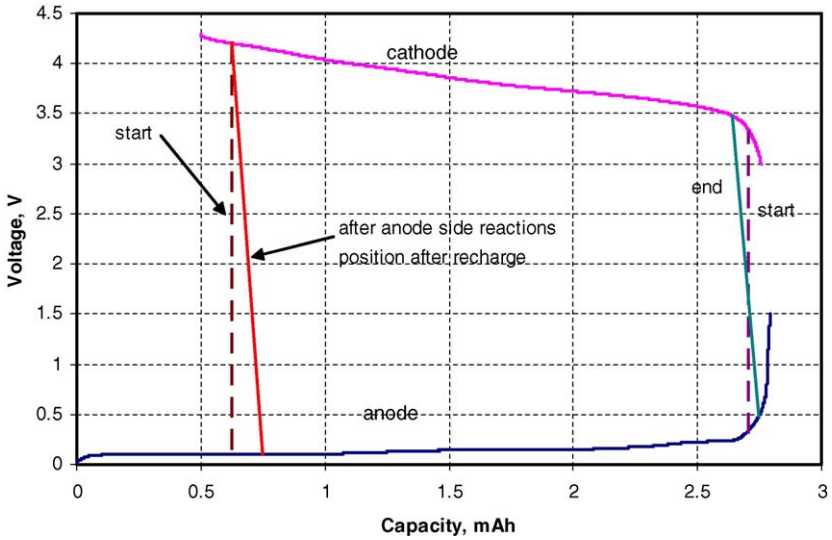

Fig. 9. Schematic illustration of the change in electrode alignment with side reactions.

mixed anode with 14–16% capacity loss in section II are the closest match.

As an example, using the $-Q_0\,dV/dQ$ curve with 14% loss of accessible capacity allows the calculation of the voltage versus capacity curve for a cell with good fidelity. As described in Ref. [2], some shifting of the voltage versus capacity curve of the data from the cathode half cell relative to the anode was needed. The cathode voltage versus capacity curve was shifted by 0.34 mAh/cm^2 relative to that of the anode. Using the voltage limits of 4.1 and 3 V to define the working capacity, a cell voltage versus capacity curve was determined from the properly aligned cathode and anode data. The derivative of the resulting cell voltage curve with respect to capacity is shown in Fig. 6 along with that from the 18650 cell. The individual cathode and anode derivatives are also included so that their contributions to the sum can be easily seen. From Fig. 6, one can see that the agreement between calculated and experimental values is very good.

Fig. 7 shows the improvement in fidelity of calculated cell discharge curves as compared to that from the 18650 cell. Curve "a" was calculated using a homogeneous anode; curve "b" using a I + II anode and curve "c" is from the 18650 cell. Comparing curves "a" and "c" shows that there are many areas where there is large separation between the curves. An example of this is in the region of 1.0–1.2 mAh/cm^2. Comparing curves "b" and "c" shows that there are smaller and fewer discrepancies between them. Thus, the agreement between calculated and experimental values is considered satisfactory.

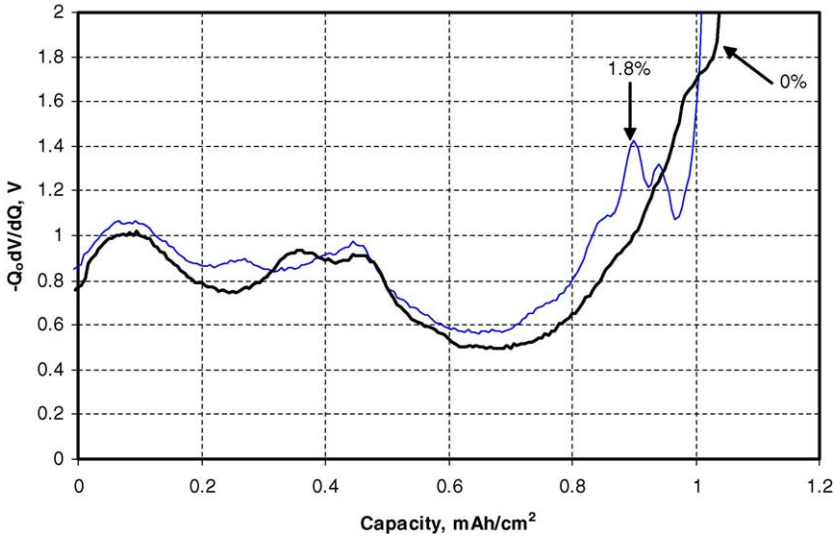

Fig. 10. Calculated $-Q_0\,dV/dQ$ vs. capacity curves for 0 and 1.8% capacity loss due to side reactions. The 0% curve is the same as that shown in Fig. 4. Notice the emergence of peaks in the region of 0.8–1 mAh/cm^2.

Returning to Fig. 2, we see that peak 3 is not as visible as peak 4 is in Fig. 1. When the cell shown in Fig. 2 ages from t = 0 to 4 weeks, peak 3 emerges from the background (Fig. 8). Additionally, the distance between peaks 2a and 3 do not change. Thus, no further loss of accessible active material is seen, yet the peaks in Fig. 8 appear to move together. Another source of capacity loss is due to side reactions.

Side reactions cause a shift in the alignment of the electrodes similar to the one used to align the electrode data in the half cells to the 18650 cell data [2]. As the alignment changes, the overall cell capacity would decrease without decreasing the capacity of either electrode. This process is illustrated schematically in Fig. 9. Before the reaction occurs, the usable capacity window, 4.1–3 V, is defined by the limits marked "start" in Fig. 9. After the side reactions occur, discharge starts at a lower spot in the anode capacity window, as indicated by the label "after anode side reactions" in the figure. The total (i.e., used + unused) anode capacity is assumed to be unaffected by these reactions. As the cell is purposely discharged, the voltage difference between the electrodes parallels the line marked "after anode side reactions" to the line marked "end". The result of this process is that, upon recharge, the anode is undercharged from its previous point. The net effect on the $-Q_0\,dV/dQ$ curves is that peaks appear and disappear at different ends of the SOC curves. In this case, anode peaks emerge at low SOC and are lost at high SOC, and vice versa for the cathode.

A calculated example of the effect of side reactions on the peak pattern of the $-Q_0\,dV/dQ$ curve is shown in Fig. 10. Here, side reactions consumed 38 μAh (~1.8% of usable capacity). The realignment of the electrodes by such a small amount of side reactions is significant, as can be seen from the figure. New peaks appear at low SOC (0.8–1.0 mAh/cm^2), and there is some shifting of the peaks at higher SOC. These observations are analogous to those seen in the 18650 cell data (Fig. 8).

Side reactions in lithium-ion cells can be beneficial or detrimental to cell performance [8]. The formation of a protective solid electrolyte interphase layer (SEI) on both the anode and cathode is an example of a beneficial side reaction process. Most of SEI layer formation happens during the initial formation process during cell assembly and qualification. Detrimental side reactions may cause the continuous consumption of active lithium without the formation of a passivating SEI layer, or may change the SEI layer. During the tests described above, the cells are heated to 45 °C. It is, therefore, possible that incomplete beneficial side reactions or acceleration of detrimental side reactions occurred at the elevated temperature. If this were to occur, one would expect to see a change in the peak pattern from the anode in the curves for t = 0 and 4 weeks, especially at low SOC. Fig. 8 shows the evidence of this process in the 18650 cell and it is interesting to note how similar Figs. 8 and 10 are. The difference between them is the amount of capacity lost in side reactions. Since the relative movement of the peaks is proportional to the amount of capacity lost, the actual cell shown in Fig. 8 lost less than the calculated one.

As the cell continues to age, further changes are seen in the plot of $-Q_0\,dV/dQ$ (see Fig. 11). As the cell ages, a new peak appears, labeled "2c" in Fig. 11. Peak 2c separates from peaks 2a and 2b as the capacity of the cell decreases. Peak 2c appears to be "fixed" at ~0.40 mAh/cm^2. Using the results from previous work [2] shows that peak 2c represents a cathode phase transition. Additionally, the peaks labeled 3 and 4 in Fig. 11 continue to emerge as the cell ages. This emergence is consistent with side reactions being the major source of capacity loss. Fig. 11 also shows that peaks 1 and 3, due to the cathode, do not move appreciably during the aging process.

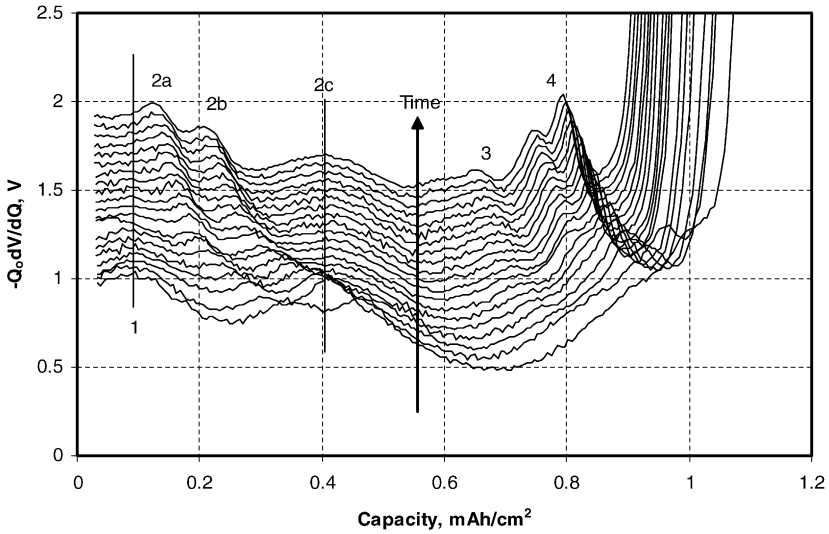

Fig. 11. Plots of $-Q_0\,dV/dQ$ vs. capacity with time for the cell depicted in Fig. 2. The time between curves is 4 weeks and a vertical offset was added for the sake of clarity. Note the new peak numbering scheme. During 76 weeks, the capacity loss was 12.9%.

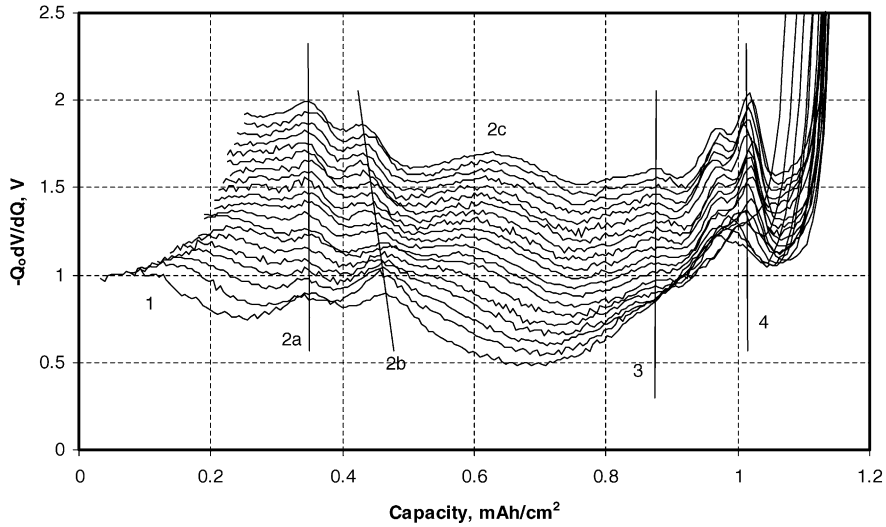

Fig. 12. Replotting the data in Fig. 11 with peak 2a aligned.

Replotting the data in Fig. 11 with peak 2a aligned in all the curves provides a different perspective on the processes occurring in the aging cell. This is shown in Fig. 12. In the figure, peaks 2a, 3 and 4 appear to be related. When there is no change in the position of peak 2a, there is also no change in the positions of peaks 4 and 5. This confirms that peaks 2a, 3, and 4 are from the same portion of the anode and peak 2b is not.

Also evident in Fig. 12 is the movement of peak 2b. It is moving toward higher SOC and, hence, toward higher cell voltage as the cell ages. A possible cause for this movement is that, due to the effect of pressure or grain alignment, some excess lithium capacity is trapped in the II portion of the anode and is not fully accessible, except under low rate conditions. Thus, the II portion appears to age at a different rate than the rest of the anode. With relatively more lithium in the II portion of the anode, it is at a slightly higher SOC and the phase transition that causes peak 2b will appear at higher cell capacities.

Thus, capacity fade in lithium-ion cells can be a complex and intertwined process. As discussed above, there are two main causes of capacity fade, loss of accessible, active material and side reactions. Which process is dominant depends on several factors, some electrochemical and some physical. Using $-Q_0\,dV/dQ$ curves to model the fade processes helps unravel which process is occurring in the life of a cell.

4. Conclusions

Analysis of $-Q_0\,dV/dQ$ curves has shown that capacity fade in high-power lithium-ion cells can be complex. From the analysis, the anode material in a significant fraction of the cells showed two types of capacity loss. The loss of accessible material tended to happen early in cell life, either during formation or during the first 4 weeks of testing. Most likely this was caused by a physical rather than chemical process. After 4 weeks, the principal cause of capacity loss was side reactions.

Acknowledgment

This work was performed under the auspices of the U.S. Department of Energy, Office of FreedomCAR and Vehicle Technologies, under contract nos. W-31-109-Eng-38 (ANL) and DE-AC07-99ID13727 (INEEL). The authors also acknowledge many fruitful discussions with Dennis W. Dees, Jun Liu, Daniel P. Abraham, and Andrew N. Jansen of ANL and with Vincent S. Battaglia of Lawrence Berkeley Laboratory.

References

[1] I. Boom, S.A. Jones, V.S. Battaglia, G.L. Henriksen, J.P. Christophersen, R.B. Wright, C.D. Ho, J.R. Belt, C.G. Motloch, J. Power Sources 538 (2003) 124.
[2] I. Bloom, A.N. Jansen, D.P. Abraham, J. Knuth, S.A. Jones, V.S. Battaglia, G.L. Henriksen, J. Power Sources 139 (2004) 295.
[3] PNGV Battery Test Manual, DOE/ID-10597, Rev. 3, February 2001.
[4] PNGV Test Plan for Advanced Technology Development Gen 2 Lithium-ion Cells, EHV-TP-121, Rev. 6, October 5, 2001.
[5] D.P. Abraham, Private communication.
[6] J.S. Gnanaraj, Y.S. Cohen, M.D. Levi, D. Aurbach, J. Electroanal. Chem. 89 (2001) 516.
[7] D. Aurbach, H. Teller, M. Koltypin, E. Levi, J. Power Sources 2 (2003) 119–121.
[8] See E. Peled, D. Golodnitsky, C. Menachem, D. Bar-Tow, J. Electrochem. Soc. 145 (1998) 3482, for a more complete discussion of the types of reactions that can occur in a lithium-ion battery.